CHEMISTRY

Reversible strain-promoted DNA polymerization

Zhenyu Han, Oliver G. Hayes, Benjamin E. Partridge, Chi Huang, Chad A. Mirkin*

Molecular strain can be introduced to influence the outcome of chemical reactions. Once a thermodynamic product is formed, however, reversing the course of a strain-promoted reaction is challenging. Here, a reversible, strain-promoted polymerization in cyclic DNA is reported. The use of nonhybridizing, single-stranded spacers as short as a single nucleotide in length can promote DNA cyclization. Molecular strain is generated by duplexing the spacers, leading to ring opening and subsequent polymerization. Then, removal of the strain-generating duplexers triggers depolymerization and cyclic dimer recovery via enthalpy-driven cyclization and entropy-mediated ring contraction. This reversibility is retained even when a protein is conjugated to the DNA strands, and the architecture of the protein assemblies can be modulated between bivalent and polyvalent states. This work underscores the utility of using DNA not only as a programmable ligand for assembly but also as a route to access restorable bonds, thus providing a molecular basis for DNA-based materials with shape-memory, self-healing, and stimuli-responsive properties.

INTRODUCTION

The discovery of strain-promoted reactions has enabled previously unidentified synthetic transformations that are efficient and selective. For instance, strained organic molecules participate in strain-promoted Diels-Alder and 1,3-dipolar cycloadditions (*1*–*3*) and strain-driven formal [1,3]-aryl shifts (*4*) and can be used to drive the synthesis of structurally complex products and react with biomolecules in living systems with high selectivity (*5*, *6*). With polymers and bulk materials, force-sensitive molecules, or mechanophores, undergo transformations, such as bond scission, isomerization, or pericyclic reactions that make materials stimuli-responsive (*7*). The reversibility of such transformations is desirable in self-healing materials, stress sensing, and additive manufacturing (*7*, *8*). However, the cleavage and rearrangement of covalent bonds are typically irreversible without the input of external energy such as heat or light. Nevertheless, this process is energetically costly, and repetitive exposure of a material to such conditions while under external stress can lead to material fatigue and failure.

DNA molecules participate in noncovalent interactions and can undergo a high degree of bending, shearing, and stretching (*9*, *10*). Mechanical rupture of DNA duplexes can be used in applications such as force sensing, mechanical regulation, and molecular recognition (*11*–*16*). In addition, colloidal crystals made from DNA-modified particles (*17*) and origami structures bonded by DNA can exhibit stimuli-responsive, elastic, and shape memory properties (*18*–*22*). However, extreme mechanical stress typically leads to the irreversible disassembly of DNA-based materials due to the mechanical unfolding of the DNA strands themselves (*20*, *23*–*27*). In the absence of stabilizing agents (*28*–*30*) or thermal annealing processes (*31*), the autonomous renaturation of assemblies bonded by multiple DNA strands is challenging due to multiple kinetic and thermodynamic barriers.

We hypothesized that assemblies composed of a minimal number of DNA strands can overcome such limitations and exhibit reversible shape recovery after force-induced disassembly. Here, we report the design and synthesis of stable cyclic DNA dimers and investigate the strain-induced, ring-opening polymerization reaction and its reversibility. The calculation of elastic potential energies provided input on the structural parameters required to synthesize cyclic dimers. Atomic force microscopy (AFM) imaging reveals that the dimers are stable. Furthermore, the differences in mechanical properties between single-stranded and double-stranded DNA are used to generate ring strain and modulate the energy landscape between the conversion of cyclic dimers and polymers. Mechanistic studies of depolymerization suggest a two-step pathway that is distinct from the ring-opening polymerization process, and reversibility is retained when a protein cargo is attached to the DNA. Overall, these findings show how DNA bonds can overcome energy barriers to revert strain-promoted reactions and enable reaction pathways and dynamic transformations that are traditionally challenging to access. When interfaced with other nanoscale building blocks, stress-responsive DNA assemblies may provide a promising route to access stimuli-responsive materials.

RESULTS

To investigate shape recovery after mechanical denaturation, we synthesized cyclic heterodimers as the minimalist structures stabilized with a pair of complementary DNA overhangs. The sticky ends were designed to be 14 nucleotides (nt) in length to ensure sufficient hybridization. While previous studies (*24*, *25*) have reported the synthesis of cyclic homodimers using 10-nt sticky ends, mixtures of monomers and dimers were found with shorter sticky ends under our experimental conditions. In addition, the nonhybridizing, single-stranded spacer region provides the structures with flexibility and does not participate in the formation of DNA rings. Together, the sequences were designed to minimize secondary structure formation and nonspecific hybridization (table S1).

When a pair of duplexer strands, complementary to the spacer regions, was added, it hybridized with the spacers to rigidify the DNA ring. Theoretically, the resulting structure should have increased ring strain and shear force at the sticky ends (Fig. 1A). Therefore, upon rigidification, the free energy of the ring increases, and the mechanical deformation of the ring leads to ring opening and subsequent polymerization (Fig. 1B). A toehold region was incorporated within the designed duplexers to allow for removal via strand

Department of Chemistry and International Institute for Nanotechnology, Northwestern University, 2145 Sheridan Road, Evanston, IL 60208, USA.
*Corresponding author. Email: chadnano@northwestern.edu

displacement (Fig. 1C). After the removal of the duplexers, the reaction products can either be retained as polymers, due to the high energetic cost of breaking the existing hybridized DNA, or revert to cyclic dimers, if the reaction is reversible.

Cyclization favored by a single unpaired nucleotide

Given the wide range of potential outcomes for the mixing of two DNA monomers containing complementary regions, a spacer design that would favor the formation of cyclic dimers over oligomers was selected. To do so, single-stranded poly(thymine) (poly-T) sequences were chosen because they are not complementary to the sticky ends and do not form secondary structures. While previous reports (*24*, *25*) used a similar poly-T design in the synthesis of homodimers, the effect of spacer length and sequences on DNA cyclization was not established in either of these systems.

To investigate the effect of spacer length on cyclization, monomers **1** and **2** (see table S1) with 0- (i.e., no spacer), 1-, 2-, 3-, 4-, 14-, 24-, and 32-nt spacers were prepared (Fig. 2A). Complementary monomers with spacers of the same length were mixed in equimolar concentrations and subjected to a slow-cooling gradient (90° to 25°C, 0.1°C/min) to obtain the thermodynamically favored structures. After cooling, reaction products were analyzed without purification using polyacrylamide gel electrophoresis (PAGE). For the 0-nt monomers, the PAGE data showed multiple bands with a range of mobilities (Fig. 2B), indicating polydisperse products. Notably, increasing the spacer length led to the disappearance of the bands for the high–molecular weight products and, with 14-nt spacers, a single band emerged as the major product. To further characterize the identity of the major product observed after spacer incorporation, a control monomer ($\mathbf{2}_{ctrl}$) was designed with the same sequence as monomer **2**, except that one sticky end (b') was replaced with a poly-T sequence of identical length (not complementary to b; fig. S1). Therefore, the only outcome of mixing monomers **1** and $\mathbf{2}_{ctrl}$ is a linear dimer with the same length as the linear dimer formed between monomers **1** and **2**, but with a slightly different sequence. In PAGE, the products of the reaction between monomers **1** and **2** (Fig. 2B, lanes 3 and 5) and monomers **1** and $\mathbf{2}_{ctrl}$ (Fig. 2B, lanes 4 and 6) had different mobilities, indicating that the major products of mixing monomers **1** and **2** were not linear dimers.

A mobility crossover point between reactions and linear controls was observed with increasing spacer length (Fig. 2B and fig. S2). Major reaction products with spacers ≤4 nt had higher mobilities than the linear dimer controls; the opposite was observed when the spacers were ≥14 nt. This observation could possibly be attributed to the differences in the molecular weight or topology of the DNA polymers. To probe the differences in the degree of oligomerization, analytical size exclusion chromatography (SEC) was used to further characterize the reactions between monomers **1** and **2** in systems with 1- and 14-nt spacers (i.e., on either side of the crossover point; Fig. 2C). The SEC profiles of the reaction mixtures showed major peaks with retention times shorter than those of the corresponding monomers, confirming the formation of oligomers with larger hydrodynamic radii. Furthermore, peaks corresponding to monomers **1** and **2** were not observed, indicating that the consumption of the starting materials was near-complete. Both reaction products exhibit longer retention times than their respective linear dimer controls, demonstrating that both products have smaller hydrodynamic radii than the analogous linear dimers. Monomers **2** and $\mathbf{2}_{ctrl}$ exhibited similar retention profiles, so this result cannot be attributed to chemical differences in these two monomers (fig. S3). Given that cyclic structures have smaller hydrodynamic radii than their linear counterparts of the same chain length (*32*), and that the products are larger than monomers, SEC data strongly support the formation of cyclic dimers. Therefore, the observed mobility crossover is due to DNA topology, which is consistent with previous reports (*32*, *33*). Compared to the linear structures, the cyclic topologies are hydrodynamically more mobile. In larger loops, however, chain entanglement becomes possible, leading to lower conformational flexibility and slower reptation during gel electrophoresis.

The extent of cyclic dimer product formation was quantified via densitometry analysis (Fig. 2D). The reaction of monomers with longer spacers favored cyclic dimer formation, and after slow cooling, spacers as short as 1 nt allowed for a ninefold increase in cyclization (63.5 ± 1.4%) compared to the 0-nt system (7.2 ± 0.4%, lowest band in Fig. 2B, lane 1). Furthermore, the yield of cyclic dimers was similar for poly-T spacers and spacers that are orthogonal to the sticky ends of monomers (scrambled sequences; table S1). To assess whether slow cooling is necessary for the generation of cyclic dimers as the major product, mixtures of monomers **1** and **2** were incubated overnight at room temperature (~22°C), and the percentage of cyclic dimer product was quantified via densitometry (fig. S4). These isothermal reactions exhibited similar product distributions to those achieved when slow cooling was used, suggesting that the formation of cyclic dimers at room temperature is thermodynamically favored.

To investigate the stabilizing role of spacers in cyclization, the elastic potential energies of cyclic dimers with varying spacer lengths were calculated using chemical potentials in equilibrium (Fig. 2E and Supplementary Text). Cyclic dimers with 1-nt spacers are found to have 2.7 K_BT less elastic energy than cyclic dimers without spacers, suggesting that 1-nt spacers mitigate the energetic penalty

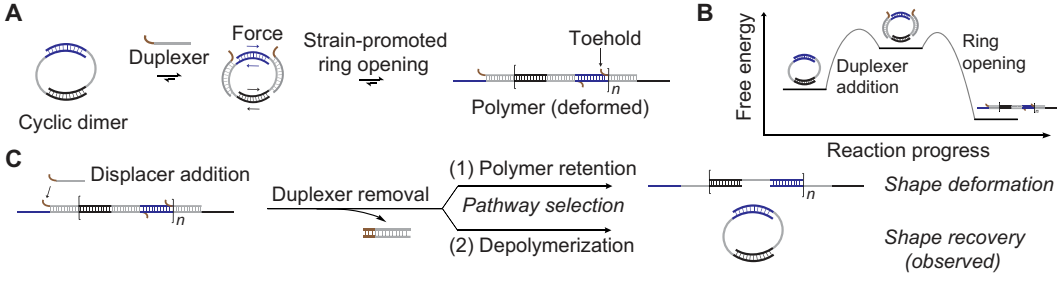

Fig. 1. Schematic showing the strain-promoted DNA polymerization. (**A**) Polymerization reaction after duplexing the nonhybridizing, single-stranded regions of cyclic dimers. (**B**) Conceptual overall free energy diagram. (**C**) Pathways of shape deformation and recovery after the removal of the strain-generating duplexers.

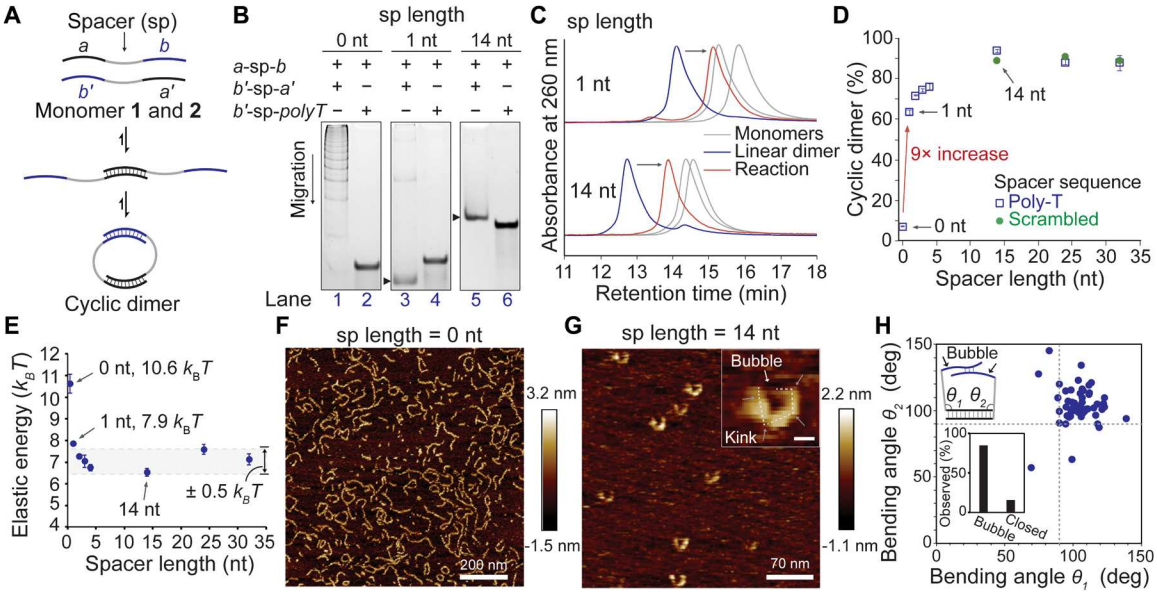

Fig. 2. Synthesis and characterization of cyclic dimers. (**A**) Reaction scheme showing monomers (top) with single-stranded DNA spacers (gray) forming linear dimers via the initial association between one pair of sticky ends (middle). Subsequent cyclization (bottom) is expected to be favored over polymerization due to the flexible spacer. (**B**) Polyacrylamide (12%) gel electrophoresis of unpurified reaction mixtures and linear dimers with 0-, 1-, and 14-nt spacers. Triangular arrows indicate the major product. (**C**) Analytical size exclusion chromatogram of reaction mixtures, linear dimers, and monomers with 1- and 14-nt spacers. (**D**) Quantification of cyclic dimers across different spacer lengths and sequences. (**E**) Calculated elastic energies of cyclic dimers as a function of spacer length. (**F**) AFM image of the reaction with 0-nt spacers. (**G**) AFM image of the reaction with 14-nt spacers along with a detailed view of a single cyclic dimer (inset). Scale bar, 10 nm (inset). (**H**) Measured bending angles and the percentage of DNA bubble formation observed using AFM.

associated with DNA bending and stretching. In addition, the elastic energies of larger (>1-nt spacer) cyclic dimers fluctuate with a much smaller amplitude of ~0.5 K_BT, indicating that the use of longer spacers contributes negligibly to the potential energy. These data suggest that a single nucleotide provides a sufficient thermodynamic driving force to form cyclic dimers by reducing ring strain. Furthermore, it is likely that one base is the minimal number needed to disrupt base stacking and provide sufficient flexibility to reduce steric hindrance in this system.

Evidence of DNA breathing

While previous work has shown that cyclic DNA is stable in the timescale of milliseconds (*34*, *35*), the cyclic dimers reported are stable over a longer timescale (days). The DNA structures were imaged using AFM in the reaction buffer [45 mM Tris (pH 8.0), 20 mM $MgCl_2$]. For the structures without spacers, polymers consisting of a mixture of cyclic and linear topologies were observed (Fig. 2F); the strain is too large to maintain them in the targeted cyclic dimer form. The cyclic oligomers exhibit curved shapes, consistent with the bending of double-stranded DNA beyond its persistence length (~50 nm) (*10*). In contrast, cyclic dimers with a 14-base spacer are connected by straight features with visible kinks and disjointed features along the closed-loop structures (Fig. 2G). Kinks, instead of smooth curved features in these cyclic structures, are observed with these structures due to the rigidity of the short DNA strands. The observed discontinuous regions are consistent with previous reports in which double-helical DNA <100 base pairs can form transient single-stranded bubbles below its melting temperature (*36*, *37*). The absence of polymeric structures over large scan areas further confirmed that the structures lacked fully accessible sticky ends for chain extension and that the formation of DNA bubbles is dynamic and temporary (fig. S5).

To understand the impact of breathing modes, we counted the number of frayed and closed loops and measured the bending angles between the fully hybridized strands for the cyclic dimers imaged (n > 50; Fig. 2H). We found a substantial amount (84%) of fraying compared to that of the fully closed structures (16%). In addition, most bending angles in these structures are >90° and are thus trapezoid-like shapes. These angles are consistently observed on the opposite sites of the fraying ends, which we attribute to transient dehybridization events that release the torsional strain and dissipate elastic energy. To further confirm the transient nature of DNA breathing, we monitored the conformations of the same cyclic dimers over four continuous AFM scan frames (fig. S6). Distinct changes in bending conformations and the interconversion between frayed and closed structures were observed over time, supporting the formation of DNA bubbles. Collectively, spacers and DNA breathing relax the bent backbones of the oligonucleotides and provide thermodynamic stability toward cyclic dimerization.

Shape recovery in strain-induced polymerization

Given that single-stranded DNA has a substantially shorter persistence length than double-stranded DNA (1.5 to 3 nm versus ~50 nm) (*25*, *38*), we hypothesized that the addition of duplexers complementary to the spacer regions of the cyclic dimers would reduce ring stability and induce ring opening by increasing the ring strain (Fig. 3A). Therefore, stoichiometric amounts of duplexers **D1** and **D2** with toehold regions were added to a solution of preformed cyclic dimers from monomers **1** and **2** bearing 24-nt spacers (Fig. 3B, lane 1). Incubation

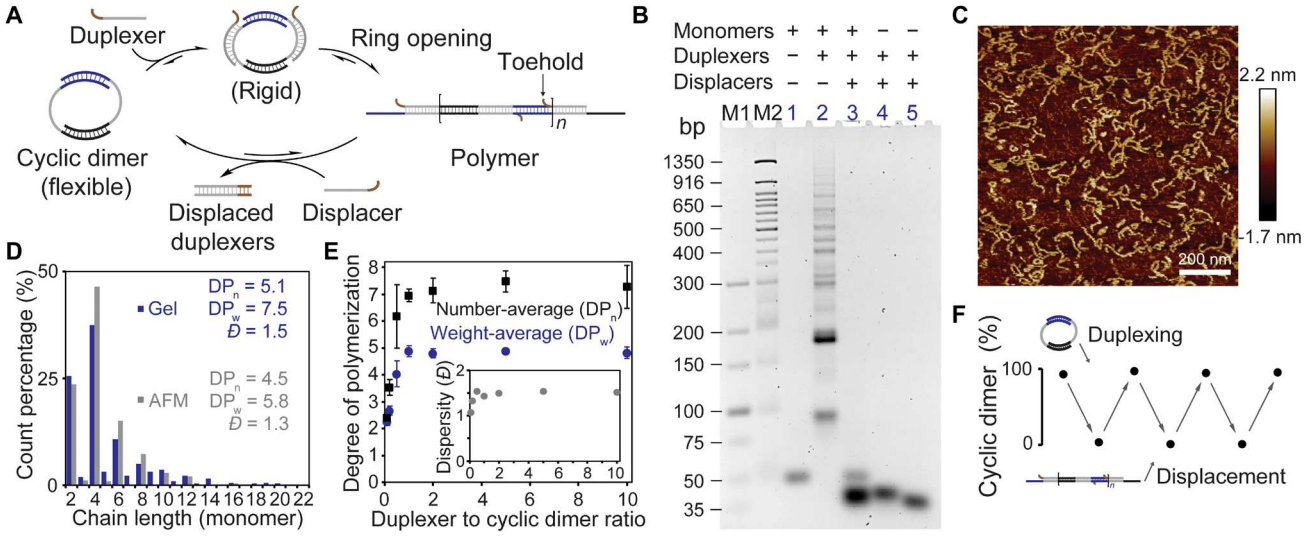

Fig. 3. Reversible strain-promoted polymerization. (**A**) Reaction scheme showing the addition of complementary duplexers to cyclic dimers containing spacers, leading to strain-promoted ring opening and polymerization. Subsequent removal of the strain-generating duplexers using toehold-mediated strand displacement drives the reaction back to cyclic dimers. (**B**) Agarose (3%) gel electrophoresis of the polymerization and recovery process. Lane 1, starting cyclic dimers with 24-nt spacers; lane 2, polymerization products after the addition of duplexers to the reaction mixture; lane 3, regenerated cyclic dimers after duplexer strand displacement; lanes 4 and 5, mixtures of duplexers with their respective complementary displacement strands, equivalent to displaced duplexers. (**C**) AFM image of polymers after ring opening. (**D**) Quantification of polymer length and degree of polymerization. (**E**) Degree of polymerization with varying ratios of duplexers added. (**F**) Yields of cyclic dimers over multiple duplexer addition and displacement cycles.

at room temperature resulted in polymerization over the course of 2 weeks (Fig. 3B, lane 2). AFM confirmed the formation of long, entangled chains with polymeric-like features along with a small subset of cyclic oligomers (Fig. 3C). Intramolecular chain termination of linear oligomers likely contributes to the formation of cyclic structures. With an equivalent number of monomeric units, cyclization results in an enthalpic gain due to the hybridization between unpaired sticky ends, which can offset the energetic penalty present due to ring strain and limited degrees of freedom (i.e., entropy) in comparison to linear counterparts. On the basis of gel results (Fig. 3B) and AFM dimension measurements, the oligomers consist of ~5 to 8 monomers from number-average (5) and weight-average (6 to 8) perspectives, respectively. The polydispersity index is 1.3 and 1.5 by AFM and gel methods, respectively (Fig. 3D). Moreover, the consumption of cyclic dimer is stoichiometric relative to the amounts of duplexers added, confirming that ring opening is driven by DNA hybridization (Fig. 3E and fig. S7). Next, to probe the reversibility of the polymerization reaction after ring opening, a stoichiometric amount of displacement strands (displacers) **D1′** and **D2′** that are fully complementary to **D1** and **D2** was added to displace the duplexers (Fig. 3A), and the system was allowed to equilibrate at room temperature for 2 weeks. Consequently, products with similar mobilities as cyclic dimers (Fig. 3B, lanes 1 and 3) were observed. This finding was rather surprising, as polymers are expected to be the thermodynamically favored products after ring opening, and depolymerization requires the dehybridization of the sticky ends, which is enthalpically costly. To test whether the polymerization-depolymerization phenomenon can be observed in more than one cycle, we repeatedly added duplexers, to rigidify cyclic dimers, and then displacers, to relax the polymers, in the same reaction mixture. The regeneration of polymers and the subsequent recovery of cyclic dimers without higher molecular weight side products over three addition and displacement cycles emphasize the reversibility of this system (Fig. 3F and fig. S8).

Depolymerization pathway

To better understand the mechanism behind the depolymerization process in this system, the kinetic and thermodynamic parameters in the hybridization and dehybridization events were explored. Given the slow kinetics of depolymerization (~2 weeks), elevated temperature conditions were explored to accelerate the rate of the reaction. Depolymerization reactions were set up at 25°, 35°, 45°, and 50°C, and the extent of each reaction was monitored by gel electrophoresis (Fig. 4A). After 1 hour of incubation, the percentage of cyclic dimer was determined to be 6 ± 1% at 25°C and elevated to 40 ± 1% and 44 ± 6% at 35°C and 45°C, respectively. Moreover, within the same time course of 1 hour, incubation at 50°C resulted in 80 ± 1% cyclic dimer products, indicating that a specific threshold of thermal energy is needed for substantial cyclic dimer conversion to occur. In addition, the extent of the recovery of cyclic dimers gradually increased over time, with the highest rate achieved at 45°C. However, the longest incubation time at 25°C produced fewer cyclic dimers than after 1 hour at 35° and 45°C, pointing to a thermodynamic barrier that can be overcome upon heating.

To characterize the formation of higher oligomers during depolymerization, we added 2 to 3 equiv of excess monomers to the reaction. Linear oligomers have unhybridized sticky ends available for chain extension through the addition of monomers (Fig. 4B). Therefore, it is expected that new products or products with enriched concentration would be observed for linear structures, and in contrast, all sticky ends in the cyclic structures would be hybridized and unable to react and the distribution of cyclic oligomers would remain the same. Given these differences in reactivity, the identification of products was pursued in chain extension experiments. A single

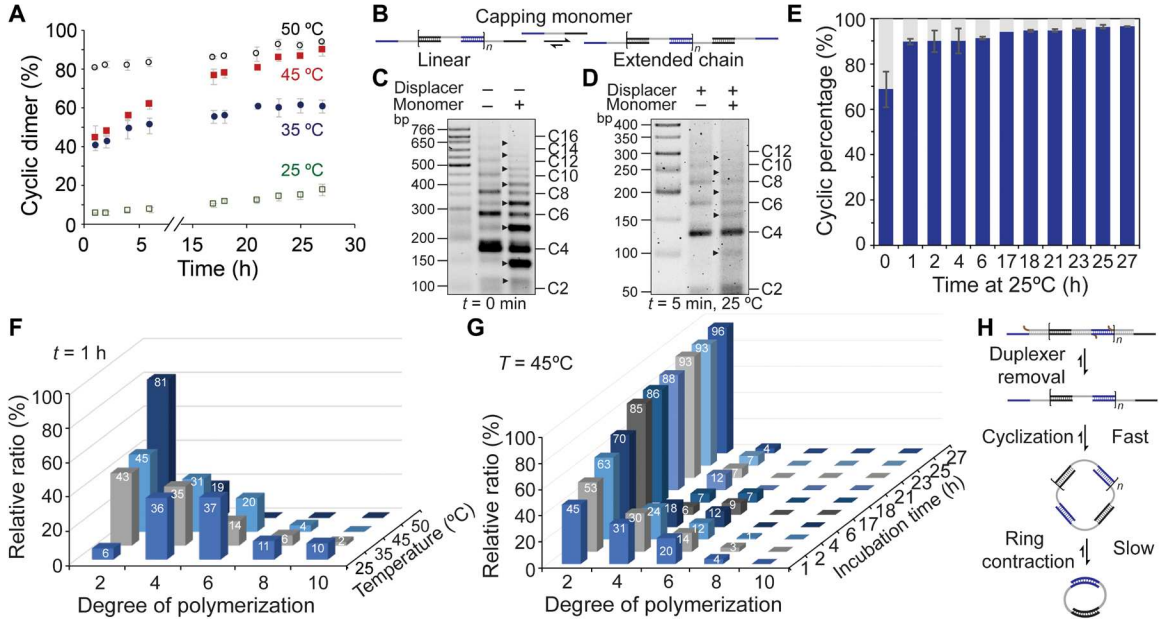

Fig. 4. Mechanistic studies of spontaneous depolymerization. (**A**) Percent yield of cyclic dimers after incubating polymers without duplexers as a function of time at various temperatures. (**B**) Scheme of chain extension reaction using linear oligomers via the addition of single monomers. Linear oligomers with either single-stranded or duplexed spacers can be extended after adding a single monomer with single-stranded or duplexed spacers, respectively. For clarity, only single-stranded spacers are shown. (**C**) Agarose (2%) gel electrophoresis of the polymerization reaction (middle) and after the addition of capping monomers with duplexed spacers (right). (**D**) Agarose (2%) gel electrophoresis of the reaction with displaced duplexers after 5 min of incubation at 25°C (middle) and the same reaction after the addition of capping monomers with single-stranded spacers (right). (C and D) Cyclic structures are identified in positions where the band intensity is relatively unchanged before and after capping. Arrows indicate the linear chains with enriched intensities on gel. (**E**) Percentage of cyclic products incubated at 25°C, over the course of 27 hours. (**F**) Relative distribution among cyclic oligomers after 1 hour at various temperatures. (**G**) Relative distribution among cyclic oligomers at 45°C, over the course of 27 hours. (**H**) Proposed two-step depolymerization route involving cyclization and ring contraction.

monomer **1** was used with the intention of forming capped polymers, as both sticky ends on the 5′ and 3′ end require the other complementary monomer **2** to continue growth. On the basis of band-shift assays, bands that correspond to cyclic and linear oligomers were identified when chain extension was performed on a polymerized sample containing duplexer strands, before the addition of displacement strands (Fig. 4C). In this assay, a monomer **1** with duplexed spacers was added to ensure that all products are hybridized with duplexers. In a separate sample, where the duplexer was displaced, the same chain extension (with unduplexed monomer **1**) was performed 5 min after the strand displacement at 25°C (Fig. 4D). Quantification via densitometry analysis revealed a drastic increase in the percentage of cyclic products in the first hour of incubation at 25°C (69 ± 8% to 90 ± 1%), despite a low yield of cyclic dimers (Fig. 4E and fig. S9). These data suggest that depolymerization after duplexer displacement proceeds initially via a rapid cyclization from linear oligomers to a distribution of cyclic oligomers.

We further analyzed the product distribution of cyclic oligomers and their conversion to cyclic dimers at different time points and temperatures. After 1 hour of depolymerization, the percentages of higher oligomers generally decreased with increasing temperature (Fig. 4F). Between 35° and 45°C, an increase in the percentage of cyclic hexamers was observed (i.e., 14 ± 1% at 35°C and 20 ± 2% at 45°C), while the percentage of cyclic dimers and tetramers remained similar at both temperatures. This observation suggests that the extra thermal energy provided at a higher temperature appears to be essential in converting cyclic octamers and decamers to smaller hexamers. In addition, cyclic dimer formation can be enriched over a longer incubation time at a set temperature (45°C; Fig. 4G). Between 17 and 21 hours, the percentage of cyclic dimers was similar, but the percentage of cyclic tetramers increased from 6 to 12%, and the percentage of cyclic hexamers decreased from 9 to 0%, indicating the conversion of hexamers to tetramers. Therefore, we propose a two-step pathway for the depolymerization process that includes cyclization and ring contraction (Fig. 4H). The cyclization of linear polymers occurs with large enthalpic gain from the hybridization of free sticky ends. Because of the large ring sizes and the flexibility of long polymers, the enthalpic cost of ring strain and the entropic cost due to the limited degree of freedom between chain ends are negligible compared to the gain in hybridization energy. The subsequent ring contraction is driven by entropy because the number of hybridization events remains the same. The enthalpic cost of temporarily breaking and reforming the sticky ends increases the energy barrier, which makes ring contraction the rate-determining step.

Reversible assemblies in protein-DNA conjugates

Given the widespread use of oligonucleotides in directing the assembly of nanomaterials (*39*, *40*), we sought to apply the structural reversibility in our system with proteins. As a proof of concept, maltose-binding protein (MBP) was used as a model protein for the attachment to DNA monomers. An MBP mutant (G353C) with a single cysteine residue on its surface was recombinantly expressed in *Escherichia coli* and purified by maltose affinity chromatography (fig. S10). The surface cysteine was subsequently functionalized with

a maleimide-modified DNA monomer **1** or **2** (Fig. 5A). The shifts in mobility by PAGE and retention time by SEC confirmed the successful preparation of monodisperse protein-DNA conjugates (figs. S10 and S11). We hypothesized that topological changes to DNA could be used to modulate the architecture and valency of MBP assemblies (Fig. 5B). Analytical SEC was used to investigate the assembly state of the protein-DNA conjugates (Fig. 5C). Monomeric protein building blocks were mixed and assembled into dimeric structures via the formation of cyclic DNA dimers. SEC revealed a decrease in retention time upon mixing, indicative of an increase in the hydrodynamic radius. The addition of duplexers **D1** and **D2** to the protein dimers resulted in products with even shorter retention times, suggesting the formation of even larger, polyvalent protein structures templated by polymeric DNA. These polydisperse products were reverted to discrete dimers by subsequent addition of displacement strands **D1′** and **D2′**. After equilibration, a product peak was observed, which had a similar retention time as that seen with the bivalent assembly. The retention times of the duplexers and displaced duplexers in the bottom two SEC profiles (Fig. 5C) match those expected for the respective DNA components (fig. S12). To visualize the architectures of the protein assemblies in these different states identified by SEC, AFM was used. Monomeric protein-DNA conjugates presented as discrete features with a height of ~2.4 nm (Fig. 5D and fig. S13), and the cross-sectional analysis of the protein dimers revealed the same height and a diameter of ~16 nm, consistent with the size of a cyclic DNA dimer as observed previously (Fig. 5E and fig. S13). Elongated chains were observed in the polyvalent state, confirming that this DNA design can template protein polymerization (Fig. 5F). A slightly lower degree of polymerization was found in protein-DNA conjugates than DNA alone, likely due to increases in steric hindrance, reduction in the DNA degrees of freedom, and changes in diffusion after protein functionalization (Fig. 5G). Together, AFM confirmed the architectures of DNA-protein monomers, dimers, and polymers. The polymerization and depolymerization of DNA-protein conjugates characterized by SEC indicate that the reversibility of DNA templates is retained when applied to a more complex biomolecular system.

DISCUSSION

Traditional strain-promoted chemistry enables new types of reactions by overcoming high energy barriers, and thus, these reactions are often irreversible after reaching a thermodynamic minimum. Here, a reversible, strain-induced polymerization reaction in DNA has been discovered by synthesizing discrete cyclic DNA dimers that build up ring strain upon subsequent rigidification. Our results show that single-stranded DNA gaps as short as a single base in length provide sufficient thermodynamic driving force for cyclization, and the breathing modes reduce the torsional strain in DNA bending. Moreover, depolymerization proceeds in these systems

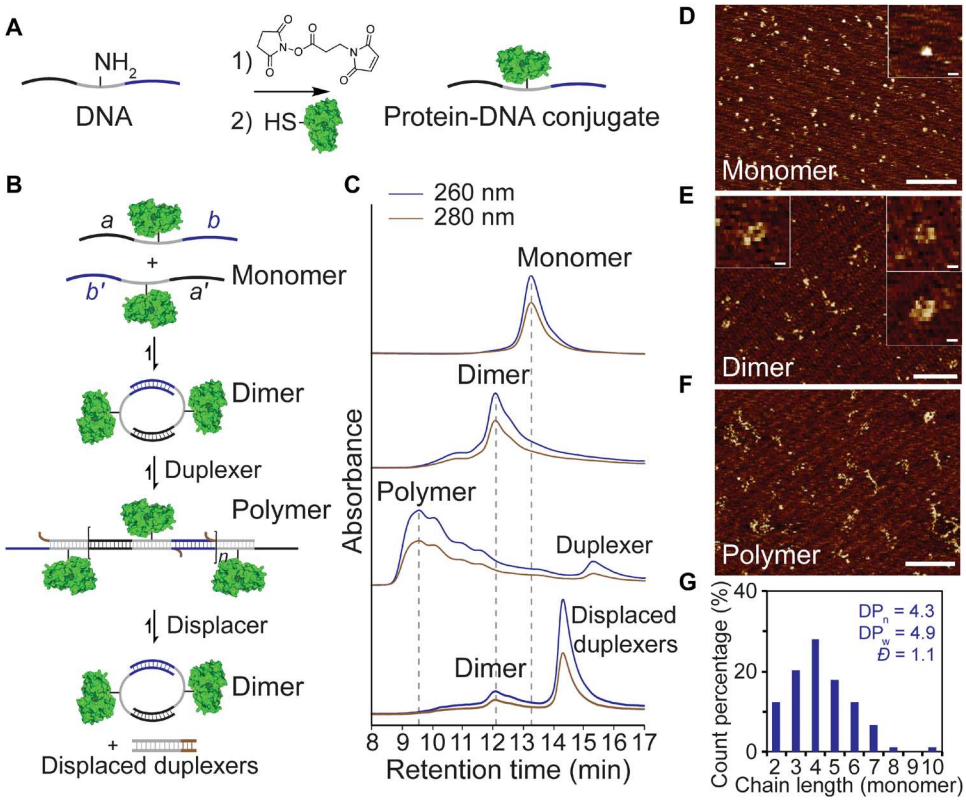

Fig. 5. Dynamic control of the oligomerization state and architectures of protein assemblies using DNA. (**A**) Synthesis of protein-DNA conjugates via an amine- and thiol-reactive bifunctional crosslinker. (**B**) Scheme for the modulation of protein assembly via duplexer addition and strand displacement. (**C**) Analytical size exclusion chromatogram for different assembly states in (B). Dashed lines are guides for the eye. (**D** to **F**) AFM images of protein-DNA conjugates in (D) monomeric, (E) dimeric, and (F) polymeric states. Scale bars, 140 nm and 10 nm (insets). (**G**) Degree of polymerization of protein-DNA conjugates.

through enthalpy-driven cyclization and entropy-driven ring contraction. The ring contraction step requires the breaking of the existing hybridization and represents a high energy barrier due to enthalpic penalty. However, the autonomous recovery of cyclic dimers after disassembly highlights the importance of reversible bonding in DNA chemistry.

Similar to the ring-opening metathesis polymerization (ROMP) of olefins (*41*), the strain-induced polymerization of cyclic DNA presented here also undergoes a chain-growth mechanism. Initiation is driven by the release of ring strain upon the addition of duplexers, the macromolecular analogs of metal alkylidene catalysts. The rapid kinetics of ring opening likely contributes to the low polydispersity ($Đ = 1.3$ to 1.5) observed in these samples. In addition, chain termination can only be realized via intramolecular cyclization or the addition of excess capping monomers. While metathesis reactions are in principle reversible, in many cases, high ceiling temperatures render depolymerization inaccessible. The design of DNA polymers that can revert back to their original cyclic dimers provides an alternative supramolecular approach to this problem.

Finally, in this design, strand displacement reactions occurred at spacer regions away from the sticky ends and served as a precise way to modulate the flexibility and strain of DNA. In principle, external application of mechanical force (e.g., using optical or magnetic tweezers) at the spacer region should also generate similar results. In addition, the demonstration that this approach can be used to deliberately reverse assembly even when the DNA is chemically carrying a biomolecular cargo, such as a protein, points to the opportunity of engineering materials with diverse stimuli-responsive and mechanical properties. Therefore, this work and these reactions should lead to DNA-based materials with applications in developing degradable polymers, adaptive biomaterials, nanomedicine agents, sensing probes, and molecular machines.

MATERIALS AND METHODS

Experimental design

We studied the reversible polymerization of cyclic DNA in the presence of ring strain. DNA sequences were designed to minimize the formation of hairpins and unintended self-dimers and heterodimers (table S1). Gel electrophoresis, AFM, and SEC were used to characterize the DNA constructs and elucidate the mechanism of the depolymerization reaction.

DNA synthesis

Oligonucleotides were synthesized in-house on UnyLinker CPG solid supports (ChemGenes), using a MerMade 12 synthesizer (BioAutomation). Standard reagents (Glen Research) and coupling procedures were used, with acetonitrilic 4,5-dicyanoimidazole as the activator and iodine as the oxidizer. For sequences with amine modifications, amino-modifier C6 dT (#10-1039, Glen Research) was used at the specified positions (table S1).

Oligonucleotides were cleaved from the solid support using standard AMA deprotection [1:1 mixture of 30% NH_4OH (aq) and 40% methylamine (aq) for 25 min at 55°C] and purified using reversed-phase high-performance liquid chromatography (HPLC) (Agilent 1260 Infinity) equipped with an Agilent Dynamax Microsorb C18 column, with a gradient of 0 to 75% acetonitrile in triethylammonium acetate buffer over 45 min. With collected fractions, dimethoxytrityl protecting groups were cleaved under 20% (v/v) acetic acid for 1 hour and lyophilized overnight. The identities of the purified oligonucleotides were confirmed by matrix-assisted laser desorption ionization mass spectrometry (MALDI MS) using a Bruker MALDI Rapiflex Tissue Typer in linear negative mode, with 2′,6′-dihydroxyacetophenone as the matrix and diammonium hydrogen citrate as the co-matrix.

Gel electrophoresis

DNA samples were prepared by mixing them at a final mass of 45 ng of DNA, 0.5 μl of glycerol, and 7 μl of 1× Tris/Borate/EDTA (TBE) buffer, run under 12% polyacrylamide gels (1× TBE for 100 min at 100 V) or agarose gels (2 or 3%, 1× TBE for 120 min at 120 V), and stained with GelRed (Biotium). Protein samples were run under 7.5% polyacrylamide gels (1× TBE for 45 min at 120 V) and stained with SimplyBlue SafeStain (Invitrogen). Denaturing protein gels were run under 4 to 15% polyacrylamide gels (1× TBE for 30 min at 200 V).

Densitometry analysis

To quantify the yield of cyclic dimers, the intensity of the bands across each gel lane was quantified via ImageJ, as reported previously (*40*, *42*). The percentage of cyclic dimers was determined as the ratio between the intensity of cyclic dimer and the total intensity of all bands.

Synthesis of cyclic and linear DNA dimers

DNA monomer stock solutions (2 μM) were prepared in 45 mM Tris (pH 8.0), 20 mM $MgCl_2$. For a typical experiment, complementary DNA monomers (monomers **1** and **2** with the same spacer designs) were combined in equal volume to obtain a final concentration of 1 μM per monomer. The linear dimer control reactions were performed by combining monomers **1** and $\mathbf{2}_{ctrl}$ of the same spacers. The combined fractions were subject to a slow-cool gradient (90° to 25°C, 0.1°C/min) using a polymerase chain reaction (PCR) thermocycler (Applied Biosystems) or allowed to react overnight (15 hours) under room temperature (22°C).

Ring-opening polymerization

For a stoichiometric reaction (Fig. 3B), 2 μl of 40 μM duplexer **D1** and 2 μl of 40 μM duplexer **D2** were added to 80 μl of annealed cyclic dimers (1 μM per monomer, with 24-nt scrambled spacers), for a total reaction volume of 84 μl. The reaction was allowed to proceed under room temperature over the course of 2 weeks. Isothermal incubation at slightly elevated temperatures led to faster reaction kinetics.

Toehold-mediated strand displacement

To 84 μl of ring-opening polymerization reaction solution, 2 μl of 40 μM duplexer complement **D1′** and 2 μl of 40 μM duplexer **D2′** were added. The reaction proceeded under room temperature or at elevated temperatures (Fig. 4) before being analyzed on a gel.

Atomic force microscopy

Samples in the assembly buffer {DNA: 45 mM Tris (pH 8.0), 20 mM $MgCl_2$; protein-DNA conjugate: 20 mM Hepes [4-(2-hydroxyethyl)-1-piperazineethanesulfonic acid, pH 7.0], 20 mM $MgCl_2$} were directly dropped onto freshly cleaved mica and incubated for 30 min at room temperature before imaging. All AFM images were captured in fluid, using PeakForce Tapping mode on a Bruker Bioscope Resolve AFM equipped with PeakForce-Hirs-F-B (Bruker). The imaging buffer was the same as the respective assembly buffer to avoid

changes in product distribution due to varying solvent or salt conditions. The effective imaging force (<80 pN) was continuously adjusted to minimize sample damage and probe manipulation. The images were flattened using NanoScope Analysis (Bruker) to remove tilt and bow. The bending angles of cyclic dimers were measured in NanoScope Analysis (Bruker). Lines were drawn over the DNA strands visualized, and the angles between strands on the opposite side of the fraying ends were measured.

Size exclusion chromatography

SEC was performed using an Agilent 1260 Infinity HPLC system equipped with Agilent Advance Bio SEC 300 Å columns. The samples were run at a flow rate of 0.5 ml/min, a temperature of 22°C, and with a mobile phase of 1× phosphate-buffered saline (PBS) (pH 7.4). Elution profiles (absorbance) were monitored at wavelengths of 260 nm and 280 nm.

Protein expression and purification

MBP (Protein Data Bank: 1MPD) genes encoding N-terminal 6× His Tag and G353C mutation were obtained from Integrated DNA Technologies and constructed in a pET28a vector using Gibson assembly. The plasmid was transformed into BL21 (DE3) electrocompetent cells (Sigma-Aldrich) via electroporation and grown on an agar plate overnight with kanamycin (50 μg/ml). Single colonies were selected to grow 7-ml cultures in LB broth, and the plasmids were extracted and submitted for Sanger sequencing. The sequencing result confirms the successful incorporation of the desired sequence (table S2).

Starter culture (7 ml) was added to 2× Yeast Extract/Tryptone/Potassium Phosphate (YTP) broth with kanamycin (50 μg/ml) and grown at 37°C to an optical density between 0.4 and 0.8, before induction with 1 mM isopropyl-β-D-thiogalactopyranoside (IPTG; Invitrogen) overnight at 20°C. The cells were spun down and resuspended in 20 mM Hepes (pH 7.0) (buffer A) and lysed using a high-pressure homogenizer. The lysate was clarified by centrifugation at 18,000*g* for 25 min, and the supernatant was loaded onto MBPTrap HP (Cytiva) pre-equilibrated with buffer A. The column was washed with five additional column volumes of buffer A, and the protein was eluted with 20 mM Hepes (pH 7.0) with 10 mM maltose (buffer B). The collected fractions were concentrated to 20 μM and kept at 4°C for conjugation reactions within a week.

Preparation of MBP-DNA conjugates

Amine-modified DNA monomers were synthesized according to general procedures, desalted, and lyophilized to dryness before use. Each DNA strand was dissolved in water to a final concentration of 1.3 mM. In total, 5.5 mg (20.8 μmol, 40 equiv) of *N*-β-maleimidopropyl-oxysuccinimide ester (BMPS; BroadPharm) was dissolved in 1200 μl of anhydrous dimethyl sulfoxide (DMSO; Thermo Fisher Scientific) and combined with 400 μl of DNA solution (0.52 μmol, 1 equiv). The reaction proceeded with 600 rpm shaking for 30 min at room temperature and was then quenched with 100 μl of 1 M Tris (pH 7.0). The unreacted crosslinker was removed by passing the reaction mixture through an Illustra NAP-25 Column (Cytiva) with buffer A as equilibrium and elution buffers. Tris(2-carboxyethyl) phosphine (TCEP) was added to the protein to a final concentration of 1 mM and incubated at room temperature for 20 min. Protein solution (2600 μl, 0.052 μmol, 0.1 equiv) was added to the maleimide-modified DNA, and the conjugation reaction proceeded with 600 rpm shaking for 15 hours at room temperature. The crude reaction mixture was concentrated and loaded onto a Macro-Prep DEAE Column (Bio-Rad). The column was washed with two column volumes of buffer A and then subjected to an elution gradient of 0 to 100% of 20 mM Hepes (pH 7.0), 1 M NaCl (buffer C) over 100 min. The protein-DNA conjugate and excess DNA typically elute over 50% buffer C, after the elution of unfunctionalized proteins. The collected fractions were then combined, concentrated, and loaded onto Profinity Ni-IMAC Cartridges (Bio-Rad) to remove excess DNA. The column was washed with five column volumes of buffer A, and then the protein-DNA conjugate was eluted under 20 mM Hepes (pH 7.0), 250 mM imidazole (buffer D). Finally, the excess imidazole was removed using ENrich SEC 650 columns (Bio-Rad), with buffer A as mobile phase. The concentration of protein-DNA conjugates was determined according to a previous method (*43*).

Assembly of MBP-DNA conjugates

MBP-DNA conjugate stock solutions (1 μM) were prepared in 20 mM Hepes (pH 7.0), 20 mM $MgCl_2$. For a typical experiment, complementary MBP-DNA conjugates were combined in equal volume to a final concentration of 0.5 μM per MBP-DNA monomer. The combined fractions were incubated overnight at room temperature or 30°C. To polymerize the proteins, 0.6 μl of 40 μM duplexers **D1** and **D2** was added to 40 μl of the assembled MBP-DNA dimer (0.5 μM per MBP-DNA monomer) to a final reaction volume of 41.2 μl and incubated overnight at 30°C. To reverse protein polymers to dimers, 0.6 μl of 40 μM duplexer complements **D1′** and **D2′** was added to 41.2 μl of protein polymer solution and incubated over 2 days at 30°C.

Supplementary Materials

This PDF file includes:

Supplementary Text
Figs. S1 to S13
Tables S1 and S2
References

REFERENCES AND NOTES

1. G. J. Bodwell, J. N. Bridson, T. J. Houghton, J. W. J. Kennedy, M. R. Mannion, 1,7-Dioxa[7](2,7)pyrenophane: The pyrene moiety is more bent than that of C70. *Chem. A Eur. J.* **5**, 1823–1827 (1999).
2. X. Zhang, M. R. Mackinnon, G. J. Bodwell, S. Ito, Synthesis of a π-extended azacorannulenophane enabled by strain-induced 1,3-dipolar cycloaddition. *Angew. Chem. Int. Ed.* **61**, e202116585 (2022).
3. Y. S. Zholdassov, L. Yuan, S. R. Garcia, R. W. Kwok, A. Boscoboinik, D. J. Valles, M. Marianski, A. Martini, R. W. Carpick, A. B. Braunschweig, Acceleration of Diels-Alder reactions by mechanical distortion. *Science* **380**, 1053–1058 (2023).
4. L. Jiang, Z. Peng, Y. Liang, Z. Tang, K. Liang, J. Liu, Z. Liu, Strain-driven formal [1,3]-aryl shift within molecular bows. *Angew. Chem. Int. Ed.* **62**, e202312238 (2023).
5. N. J. Agard, J. A. Prescher, C. R. Bertozzi, A strain-promoted [3 + 2] azide–alkyne cycloaddition for covalent modification of biomolecules in living systems. *J. Am. Chem. Soc.* **126**, 15046–15047 (2004).
6. A. V. Kelleghan, A. S. Bulger, D. C. Witkowski, N. K. Garg, Strain-promoted reactions of 1,2,3-cyclohexatriene and its derivatives. *Nature* **618**, 748–754 (2023).
7. J. Li, C. Nagamani, J. S. Moore, Polymer mechanochemistry: From destructive to productive. *Acc. Chem. Res.* **48**, 2181–2190 (2015).
8. M. A. Ghanem, A. Basu, R. Behrou, N. Boechler, A. J. Boydston, S. L. Craig, Y. Lin, B. E. Lynde, A. Nelson, H. Shen, D. W. Storti, The role of polymer mechanochemistry in responsive materials and additive manufacturing. *Nat. Rev. Mater.* **6**, 84–98 (2021).
9. H. Qu, C.-Y. Tseng, Y. Wang, A. J. Levine, G. Zocchi, The elastic energy of sharply bent nicked DNA. *Europhys. Lett.* **90**, 18003 (2010).

10. S. B. Smith, Y. Cui, C. Bustamante, Overstretching B-DNA: The elastic response of individual double-stranded and single-stranded DNA molecules. *Science* **271**, 795–799 (1996).
11. P. C. Nickels, B. Wünsch, P. Holzmeister, W. Bae, L. M. Kneer, D. Grohmann, P. Tinnefeld, T. Liedl, Molecular force spectroscopy with a DNA origami–based nanoscopic force clamp. *Science* **354**, 305–307 (2016).
12. H. Li, C. Zhang, Y. Hu, P. Liu, F. Sun, W. Chen, X. Zhang, J. Ma, W. Wang, L. Wang, P. Wu, Z. Liu, A reversible shearing DNA probe for visualizing mechanically strong receptors in living cells. *Nat. Cell Biol.* **23**, 642–651 (2021).
13. Y. Hu, Y. Duan, K. Salaita, DNA nanotechnology for investigating mechanical signaling in the immune system. *Angew. Chem. Int. Ed.* **62**, e202302967 (2023).
14. E. Del Grosso, G. Ragazzon, L. J. Prins, F. Ricci, Fuel-responsive allosteric DNA-based aptamers for the transient release of ATP and cocaine. *Angew. Chem. Int. Ed.* **58**, 5582–5586 (2019).
15. R. Saran, Y. Wang, I. T. S. Li, Mechanical flexibility of DNA: A quintessential tool for DNA nanotechnology. *Sensors* **20**, 7019 (2020).
16. D. Mariottini, A. Idili, M. A. D. Nijenhuis, T. F. A. De Greef, F. Ricci, DNA-based nanodevices controlled by purely entropic linker domains. *J. Am. Chem. Soc.* **140**, 14725–14734 (2018).
17. C. A. Mirkin, R. L. Letsinger, R. C. Mucic, J. J. Storhoff, A DNA-based method for rationally assembling nanoparticles into macroscopic materials. *Nature* **382**, 607–609 (1996).
18. S. Lee, H. A. Calcaterra, S. Lee, W. Hadibrata, B. Lee, E. Oh, K. Aydin, S. C. Glotzer, C. A. Mirkin, Shape memory in self-adapting colloidal crystals. *Nature* **610**, 674–679 (2022).
19. M. R. Jones, N. C. Seeman, C. A. Mirkin, Programmable materials and the nature of the DNA bond. *Science* **347**, 1260901 (2015).
20. J. Ji, D. Karna, H. Mao, DNA origami nano-mechanics. *Chem. Soc. Rev.* **50**, 11966–11978 (2021).
21. C. R. Laramy, M. N. O'Brien, C. A. Mirkin, Crystal engineering with DNA. *Nat. Rev. Mater.* **4**, 201–224 (2019).
22. Y. Li, R. Schulman, DNA nanostructures that self-heal in serum. *Nano Lett.* **19**, 3751–3760 (2019).
23. Y. Duan, R. Glazier, A. Bazrafshan, Y. Hu, S. A. Rashid, B. G. Petrich, Y. Ke, K. Salaita, Mechanically triggered hybridization chain reaction. *Angew. Chem. Int. Ed.* **60**, 19974–19981 (2021).
24. Z. Zhang, S. Yu, H. Zuo, DNA ring-opening polymerization driven by base stacking. *Chembiochem* **22**, 1621–1626 (2021).
25. H. Jia, J. Shi, W. Ren, J. Zhao, Y. Dong, D. Liu, Controllable supramolecular "ring opening" polymerization based on DNA duplex. *Polymer* **171**, 121–126 (2019).
26. A. Wang, G. Zocchi, Elastic energy driven polymerization. *Biophys. J.* **96**, 2344–2352 (2009).
27. M. C. Engel, D. M. Smith, M. A. Jobst, M. Sajfutdinow, T. Liedl, F. Romano, L. Rovigatti, A. A. Louis, J. P. K. Doye, Force-induced unravelling of DNA origami. *ACS Nano* **12**, 6734–6747 (2018).
28. Z. Li, L. Liu, M. Zheng, J. Zhao, N. C. Seeman, C. Mao, Making engineered 3D DNA crystals robust. *J. Am. Chem. Soc.* **141**, 15850–15855 (2019).
29. T. Gerling, M. Kube, B. Kick, H. Dietz, Sequence-programmable covalent bonding of designed DNA assemblies. *Sci. Adv.* **4**, eaau1157 (2018).
30. E. Auyeung, R. J. Macfarlane, C. H. J. Choi, J. I. Cutler, C. A. Mirkin, Transitioning DNA-engineered nanoparticle superlattices from solution to the solid state. *Adv. Mater.* **24**, 5181–5186 (2012).
31. E. Auyeung, T. I. N. G. Li, A. J. Senesi, A. L. Schmucker, B. C. Pals, M. O. de la Cruz, C. A. Mirkin, DNA-mediated nanoparticle crystallization into Wulff polyhedra. *Nature* **505**, 73–77 (2014).
32. F. M. Haque, S. M. Grayson, The synthesis, properties and potential applications of cyclic polymers. *Nat. Chem.* **12**, 433–444 (2020).
33. R. An, Q. Li, Y. Fan, J. Li, X. Pan, M. Komiyama, X. Liang, Highly efficient preparation of single-stranded DNA rings by T4 ligase at abnormally low Mg(II) concentration. *Nucleic Acids Res.* **45**, e139 (2017).
34. R. Vafabakhsh, T. Ha, Extreme bendability of DNA less than 100 base pairs long revealed by single-molecule cyclization. *Science* **337**, 1097–1101 (2012).
35. T. E. Cloutier, J. Widom, Spontaneous sharp bending of double-stranded DNA. *Mol. Cell* **14**, 355–362 (2004).
36. C. Phelps, W. Lee, D. Jose, P. H. Von Hippel, A. H. Marcus, Single-molecule FRET and linear dichroism studies of DNA breathing and helicase binding at replication fork junctions. *Proc. Natl. Acad. Sci. U.S.A.* **110**, 17320–17325 (2013).
37. J. Yan, J. F. Marko, Localized single-stranded bubble mechanism for cyclization of short double helix DNA. *Phys. Rev. Lett.* **93**, 108108 (2004).
38. Q. Chi, G. Wang, J. Jiang, The persistence length and length per base of single-stranded DNA obtained from fluorescence correlation spectroscopy measurements using mean field theory. *Phys. A Stat. Mech. Appl.* **392**, 1072–1079 (2013).
39. J. R. McMillan, O. G. Hayes, J. P. Remis, C. A. Mirkin, Programming protein polymerization with DNA. *J. Am. Chem. Soc.* **140**, 15950–15956 (2018).
40. C. A. Figg, P. H. Winegar, O. G. Hayes, C. A. Mirkin, Controlling the DNA hybridization chain reaction. *J. Am. Chem. Soc.* **142**, 8596–8601 (2020).
41. S. Sutthasupa, M. Shiotsuki, F. Sanda, Recent advances in ring-opening metathesis polymerization, and application to synthesis of functional materials. *Polym. J* **42**, 905–915 (2010).
42. C. A. Schneider, W. S. Rasband, K. W. Eliceiri, NIH Image to ImageJ: 25 years of image analysis. *Nat. Methods* **9**, 671–675 (2012).
43. J. R. McMillan, C. A. Mirkin, DNA-functionalized, bivalent proteins. *J. Am. Chem. Soc.* **140**, 6776–6779 (2018).

Acknowledgments: We would like to thank Y. Gu for helpful discussions. This work made use of the SPID facilities of the NUANCE Center and IMSERC at Northwestern University, which have received support from Soft and Hybrid Nanotechnology Experimental (SHyNE) Resource (NSF-ECCS-1542205), MRSEC program (NSF DMR-1121262) at the Materials Research Center, the International Institute for Nanotechnology (IIN), the Keck Foundation, and the State of Illinois. **Funding:** This material is based upon work supported by the following awards: National Science Foundation DMR-2104353, Air Force Office of Scientific Research FA9550-22-1-0300, and the Sherman Fairchild Foundation Inc. **Author contributions:** Conceptualization: Z.H., O.G.H., B.E.P., C.H., and C.A.M. Methodology, investigation, and visualization: Z.H. Supervision: C.A.M. Writing—original draft: Z.H. Writing—review and editing: Z.H., O.G.H., B.E.P., C.H., and C.A.M. **Competing interests:** The authors declare that they have no competing interests. **Data and materials availability:** All data needed to evaluate the conclusions in the paper are present in the paper and/or the Supplementary Materials.

Submitted 21 February 2024
Accepted 20 March 2024
Published 24 April 2024
10.1126/sciadv.ado8020